RESEARCH ARTICLE | MARCH 03 2022

Numerical simulation on transportation behavior of dense coarse particles in vertical pipe with an optimized Eulerian–Lagrangian method

Yan Zhang (张岩) ; Xiao-Bing Lu (鲁晓兵) ; Xu-Hui Zhang (张旭辉) ✉

Physics of Fluids 34, 033305 (2022)
https://doi.org/10.1063/5.0084263

Physics of Fluids ARTICLE scitation.org/journal/phf

Numerical simulation on transportation behavior of dense coarse particles in vertical pipe with an optimized Eulerian–Lagrangian method

Cite as: Phys. Fluids 34, 033305 (2022); doi: 10.1063/5.0084263
Submitted: 5 January 2022 · Accepted: 14 February 2022 ·
Published Online: 3 March 2022

Yan Zhang (张岩), Xiao-Bing Lu (鲁晓兵), and Xu-Hui Zhang (张旭辉)[a]

AFFILIATIONS

Institute of Mechanics, Chinese Academy of Sciences, Beijing 100190, China

[a]Author to whom correspondence should be addressed: zhangxuhui@imech.ac.cn

ABSTRACT

Solid–liquid two-phase flow with dense coarse particles in the pipeline exists widely in energy and resources engineering, especially in the prospective hydraulic lifting scenario of deep-sea mining. In this paper, the coarse particles' transportation behavior in a vertical pipe is investigated based on an optimized Eulerian–Lagrangian method proposed in our previous work. The coarse particle transportation in the vertical pipe is characterized as multi-processes and multi-physical effects and is not fully captured due to the limitations on experimental apparatus, experimental measurement techniques, and numerical simulation techniques. Little research has been done on the local characteristics of the flow and their effect on the hydraulic lifting performance. The characteristics of the internal flow field, particle retention, and hydraulic lifting efficiency are disturbed under the condition of the continuous supply with the constant inlet two-phase concentration and velocity. The simulation results illustrate that particle transportation process can be roughly divided into three stages, single phase flow stage, mixing stage, and stable transportation stage, and shows a dilute-dense non-continuous flow pattern due to particle retention. Based on parametric studies, the retention phenomenon is alleviated by the increase in the water inlet velocity and almost disappears at approximately 12 000 of the Reynolds number, where the flow pattern transition occurs. Finally, the hydraulic lifting performance, such as a critical lifting condition and the friction loss, is analyzed and the transition of flow pattern is discussed.

I. INTRODUCTION

Solid–liquid two-phase flow with coarse particles in the pipeline exists widely in energy and resources engineering,[1–4] such as the coal and mining industries,[5–10] the gas hydrates exploitation,[11–13] and so on. For example, deep-sea mineral resources have attracted considerable attention due to increased energy demand in various countries.[14,15] The hydraulic lifting is currently the most promising mining method for offshore mineral resources with benefits of high recovery rate, high productivity, and practical operation.[4] The manganese nodules on the deep sea bottom are transported to the mining ship moored at sea level through a hydraulic lifting system, which is shown in Fig. 1. The internal flow through the pipeline contains seawater and nodules, which is a typical dense two-phase mixed flow.

Nodule particles are estimated to be in the range of tens of millimeters.[16] According to Cúñez *et al.*[17] and Cúñez and Franklin,[18] different flow instabilities and patterns have been identified for the solid-liquid two-phase flow with coarse particles ($d/D > 0.1$, where d/D is the ratio of particle diameter to pipe diameter). The transportation of coarse particles in the pipeline requires careful consideration of numerous factors, such as the particle concentration, particle and water properties, particle diameter, as well as particle–water, particle–particle, and particle–wall interactions.[19] The motion characteristics, flow resistance, and stable transport law of two-phase solid–liquid flow with dense coarse particles in the pipeline are the key basis for optimizing hydraulic lifting programs. Due to the limitations on observation and modeling of dense coarse particles' flow behaviors, the satisfactory progress is challenging. In engineering practice of transportation, the lifting distance can reach hundreds to thousands of meters. Limited information such as the flow rates and pressure difference can be obtained by using some sensors in the pipe. However, it is of great difficulties in monitoring the flow behaviors. In addition, numerical simulation of the transportation process in such a long pipeline is limited by the high computational cost. Hence, laboratory test or numerical simulation in a moderate small scale is usually adopted. In previous work, rich results were obtained on the flow characteristics of fine suspended particulates in water.[20–27]

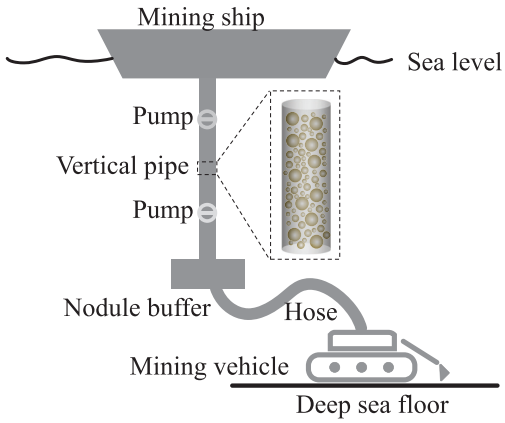

FIG. 1. Sketch of the hydraulic lifting method.

However, the ratio of coarse particles to pipeline diameter is around 0.1–0.2. It poses a challenge to efficient and stable transportation to meet the operational requirements of coarse and fine particle mixing and continuous large-scale transportation (without blockage or flow instabilities). To address the problem of hydraulic lifting of coarse particles, many researchers investigated the minimum lifting velocity of particles with a single particle diameter (5–50 mm),[28] the settling velocity of coarse particle clusters,[29] two-phase flow characteristics,[30] and the influence of particle shape on the hydraulic lifting process[31] through experimental and numerical simulation methods, and proposed the optimization parameters required for stable transportation in hydraulic lifting process. The effect of particle concentration, pipeline diameter, water velocity, and other factors on the radial particle distribution within the pipe has been achieved.[4,7,32,33] In addition, the flow assurance is also important for the hydraulic lifting. It is found that irregularly shaped coarse particles and higher particle concentration increase the possibility of particle blockage in the pipeline.[31] Through a combination of theoretical analysis and laboratory experiments, Van Wijk *et al.*[34,35] investigated the possible blockage caused by fine particles bypassing coarse particles when transporting solid–liquid mixtures with particles of a certain size distribution. They established a frictional stress model between the solid–liquid mixture and the pipe wall by drawing on the theory of internal friction angle and friction coefficient of geotechnics.

The coarse particles' transportation in the vertical pipe is characterized as multi-processes and multi-physical effects and is not fully captured due to the limitations on experimental apparatus, experimental measurement techniques, and numerical simulation techniques. Current research on the hydraulic lifting of coarse particles is still immature and needs to be investigated further for capturing more information on the flow field and the motion feature of the particles. For example, the local characteristics of the flow in the continuous lifting process is still not fully understood, mainly because less attention is paid to the changing characteristics of the flow field in engineering, and the current experimental measurement techniques are difficult to achieve the local characteristics of the flow in the pipeline, such as local concentration, velocity, and flow field. In addition, there are a few studies on the analysis of the hydraulic lifting performance, such as the lack of common and simple relationships for predicting local parameters and the lack of formula for calculating critical hydraulic lifting velocity. Therefore, it is necessary to reveal the flow mechanism of the solid–liquid flow with coarse particles and to clarify the main control factors and the regularity of the internal flow.

In general, for most industrial-scale solid–fluid coupling systems, including hydraulic lifting in deep-sea mining mentioned above or proppant transport in petroleum engineering, three characteristic scales exist:[36,37] microscale, mesoscale, and microscale. Corresponding appropriate numerical approaches are available to investigate the two-phase flow characteristics for each scale. At the macroscale, the macroscopic motion behavior of the two-phase flow is focused on, where variables of both the two phases are obtained by solving locally averaged Eulerian transport equation.[38,39] For simulating particles at the micro-scale, we track individual particles trajectories by calculating their instant velocities; the latter velocities are calculated via solving Newton's law.[40] The forces on particle are obtained by the surface integral of the particle and the non-slip boundary condition is fulfilled at the particle surface. Hence, this method is also called particle-resolved direct numerical simulation (PR-DNS). At the meso-scale, point particle model is used for the solid–liquid interaction, where the interaction forces are calculated based on force models and the non-slip boundary condition is not fulfilled at the particles surface. In our previous work, a review of numerical methods describing solid–liquid two-phase flows was given, and the capabilities of various numerical approaches were summarized.[37] The macroscale simulation methods, such as the two-fluid model (TFM),[41] are widely used in engineering designs due to low computational cost. However, the microscale and mesoscale behaviors of the hydraulic lifting process are also crucial for engineering designs such as the particle–particle interactions, particle sizes, and the particle composition.

In this work, an optimized Eulerian–Lagrangian method proposed in our previous work[37] is utilized to elucidate the solid–liquid two-phase flow with coarse particles in a vertical pipe based on the background of the hydraulic lifting process in deep-sea mining. On the one hand, we intend to illustrate the local characteristics of the particles, such as the particle retention. On the other hand, we aim to analyze the two-phase flow field characteristics in the vertical pipe and the hydraulic lifting performance. The previous work presents a suitable method for the numerical simulation of the solid–liquid two-phase flow with coarse particles, addressing the hydraulic lifting process of dense coarse particles.

The remainder of this paper is as follows: in Sec. II, a short recapitulation is given to summarize the numerical model, such as the governing equations of fluid and solid phases, fluid–particle coupling force, and numerical issues. In Sec. III, the model is validated by an experiment. In Sec. IV, problem and numerical settings for the coarse particles transportation in a vertical pipe are described. Section V focuses mainly on the local particles characteristics and the two-phase flow field. Finally, conclusions are drawn in Sec. VI.

II. MODEL DESCRIPTION

A. Solid phase equations

The translation and rotation of each particle can be calculated by the following equations based on Newton's second law:[42]

$$m\frac{\mathrm{d}\mathbf{v}}{\mathrm{d}t} = \mathbf{F}_{\mathrm{pf}} + \mathbf{F}_{\mathrm{c}} + m\mathbf{g}, \tag{1}$$

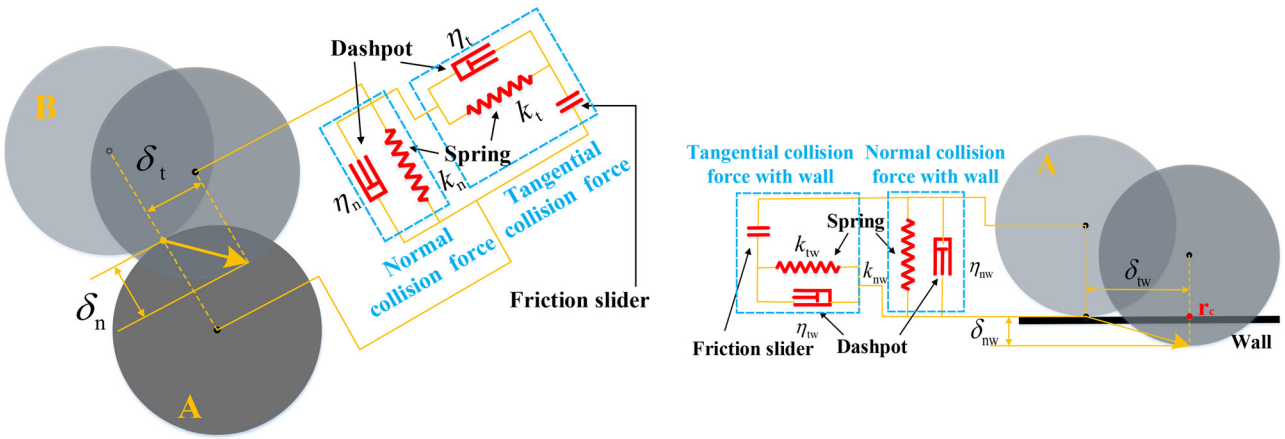

FIG. 2. The diagram of the soft particle model: (a) collision between two particles and (b) collision between a particle and a wall.

$$I\frac{\mathrm{d}\boldsymbol{\omega}}{\mathrm{d}t}=\mathbf{M}, \tag{2}$$

where m, $\mathbf{v}$, $I=md^2/10$, and $\boldsymbol{\omega}$ are the particle mass, translation velocity, the moment of inertia, and angular velocity; d is the particle diameter; $\mathbf{F}_{\mathrm{pf}}$ is the particle–fluid interaction force such as the drag force and pressure gradient force; $\mathbf{F}_{\mathrm{c}}$ is the contact force; $\mathbf{g}$ is the gravity acceleration; and $\mathbf{M}$ indicates the friction torque. The contact force can be decomposed into normal $\mathbf{F}_{\mathrm{cn}}$ and tangential $\mathbf{F}_{\mathrm{ct}}$ components and is calculated based on the soft model,[43] which is shown in Fig. 2. The soft model refers to the fact that particles can deform during a contact and the deformation is taken into account in force models.

The normal component $\mathbf{F}_{\mathrm{cn}}$ is defined as

$$\mathbf{F}_{\mathrm{cnB}\to\mathrm{A}}=\left(k_{\mathrm{n}}\delta_{\mathrm{n}}^{\frac{3}{2}}-\eta_{\mathrm{n}}\mathbf{v}_{\mathrm{AB}}\cdot\mathbf{n}\right)\mathbf{n}, \tag{3}$$

and the tangential component $\mathbf{F}_{\mathrm{ct}}$ is defined as

$$\mathbf{F}_{\mathrm{ctB}\to\mathrm{A}}=\begin{cases}k_{\mathrm{t}}|\boldsymbol{\delta}_{\mathrm{t}}|>\mu\mathbf{F}_{\mathrm{cnB}\to\mathrm{A}}, & -\mu|\mathbf{F}_{\mathrm{cnB}\to\mathrm{A}}|\dfrac{\mathbf{v}_{\mathrm{slipAB}}}{|\mathbf{v}_{\mathrm{slipAB}}|},\\ k_{\mathrm{t}}|\boldsymbol{\delta}_{\mathrm{t}}|\le\mu\mathbf{F}_{\mathrm{cnB}\to\mathrm{A}}, & -k_{\mathrm{t}}\boldsymbol{\delta}_{\mathrm{t}}-\eta_{\mathrm{t}}\mathbf{v}_{\mathrm{slipAB}},\end{cases} \tag{4}$$

where $\mathbf{F}_{\mathrm{cnB}\to\mathrm{A}}$ and $\mathbf{F}_{\mathrm{ctB}\to\mathrm{A}}$ are the contact force (normal and tangential component) of particle B to particle A, respectively. n and t represent the normal and tangential directions, and k, η, and $\boldsymbol{\delta}$ are the spring coefficient, the damping coefficient, and the particle deformation or particle overlaps, respectively. μ is the friction coefficient. More details about the soft model can be found in Refs. 25 and 44.

B. Fluid phase equations

The fluid phase motion is governed by the volume-averaged incompressible Navier–Stokes (N–S) equation[37]

$$\frac{\partial\alpha_{\mathrm{f}}}{\partial t}+\nabla\cdot(\alpha_{\mathrm{f}}\mathbf{u})=0, \tag{5}$$

$$\begin{aligned}&\frac{\partial}{\partial t}(\alpha_{\mathrm{f}}\mathbf{u})+\nabla\cdot(\alpha_{\mathrm{f}}\mathbf{u}\mathbf{u})-\mathbf{u}\left(\frac{\partial\alpha_{\mathrm{f}}}{\partial t}+\nabla\cdot(\alpha_{\mathrm{f}}\mathbf{u})\right)-\nabla\cdot(\alpha_{\mathrm{f}}\boldsymbol{\tau}_{\mathrm{f}})\\&\quad=-\alpha_{\mathrm{f}}\nabla\frac{P_{\mathrm{rgh}}}{\rho_{\mathrm{f}}}-\left(\alpha_{\mathrm{f}}\frac{\rho}{\rho_{\mathrm{f}}}-1\right)\mathbf{g}-\frac{\alpha_{\mathrm{f}}}{\rho_{\mathrm{f}}}\mathbf{g}\cdot\mathbf{h}\nabla\rho-\frac{\mathbf{f}_{\mathrm{p}}}{\rho_{\mathrm{f}}},\end{aligned} \tag{6}$$

where α_{f} is the volume fraction of the fluid, $\mathbf{u}$ is the mass-averaged fluid velocity, $\rho=\alpha_{\mathrm{f}}\rho_{\mathrm{f}}+(1-\alpha_{\mathrm{f}})\rho_{\mathrm{p}}$ is the mixture density, ρ_{f} and ρ_{p} are the fluid and particle density, respectively. $\boldsymbol{\tau}_{\mathrm{f}}$ is the viscous stress tensor of the fluid, $\mathbf{f}_{\mathrm{p}}$ is the source term describing momentum transfer between the solid phase and the fluid phase, $\mathbf{h}$ is the position vector, $P_{\mathrm{rgh}}=P-\rho\mathbf{g}\cdot\mathbf{h}$ is the relative motion pressure, which is used to make the definition of boundary conditions easier as well as to reduce the false velocity caused by hydrostatic pressure under non-orthogonal grids,[45] and P is the fluid pressure. The third term of the left-hand side of Eq. (6) can help to maintain the boundedness of the solution variable and promote better convergence.[46,47] The viscous stress tensor of the fluid is expressed as

$$\boldsymbol{\tau}_{\mathrm{f}}=\nu_{\mathrm{f}}(\nabla\mathbf{u}+\nabla\mathbf{u}^{\mathrm{T}})-\frac{2}{3}\nu_{\mathrm{f}}\nabla\cdot\mathbf{u}\mathbf{I}, \tag{7}$$

where ν_{f} is the kinematic viscosity of the fluid phase and $\mathbf{I}$ is the identity matrix. The Reynolds-averaged Navier-Stokes (RANS) $k-\varepsilon$ model is used for the fluid phase but the turbulence modulation by particles is ignored, as done from previously researchers' work.[48–50]

C. Fluid–solid interaction

The fluid–solid interaction force exerted on a particle can be modeled as a combination of drag force, pressure gradient force, virtual mass force, Basset force, and other force.[2] The drag force, the pressure gradient force, and the virtual mass force are most important in the solid–liquid two-phase flow with coarse particles.[37] Therefore, in this work, we consider the above three forces for fluid–solid interaction, which can be expressed as

$$\mathbf{F}_{pf} = \mathbf{F}_d + \mathbf{F}_p + \mathbf{F}_v, \tag{8}$$

where $\mathbf{F}_d$ is the drag force, $\mathbf{F}_p$ is the pressure gradient force, and $\mathbf{F}_v$ is the virtual mass force.

The drag force is important and is given based on the EugunWenYu model[51]

$$\mathbf{F}_d = k_d(\mathbf{u} - \mathbf{v}), \tag{9}$$

$$k_d = \begin{cases} \alpha_f < 0.8 & V_p\left(150\dfrac{(1-\alpha_f)}{\alpha_f}\dfrac{\mu_f}{d^2} + 1.75\dfrac{\rho_f|\mathbf{u}-\mathbf{v}|}{d}\right), \\ \alpha_f \geq 0.8 & V_p\dfrac{3}{4}C_d\dfrac{\rho_f|\mathbf{u}-\mathbf{v}|}{d}\alpha_f^{-2.65}, \end{cases} \tag{10}$$

$$C_d = \begin{cases} Re < 1000 & \dfrac{24(1+0.15Re^{0.687})}{Re}, \\ Re \geq 1000 & 0.424, \end{cases} \tag{11}$$

$$Re = \frac{\rho_f|\mathbf{u}-\mathbf{v}|d}{\mu_f}, \tag{12}$$

where k_d is the momentum transfer coefficient between different phases, V_p is the particle volume, C_d is the drag coefficient, Re is the relative particle Reynolds number, and μ_f is the viscosity of the fluid phase.

The pressure gradient force and the virtual mass force are calculated from the fluid field

$$\mathbf{F}_p = -V_p\nabla P, \tag{13}$$

$$\mathbf{F}_v = -\frac{\rho_f V_p}{2}\left(\frac{D\mathbf{u}}{Dt} - \frac{d\mathbf{v}}{dt}\right), \tag{14}$$

where $D\mathbf{u}/Dt$ is the material derivative of the fluid.

D. Optimization treatment

The optimization treatment of this method is briefly illustrated here. First, the barycentric coordinates are introduced into the particle localization in this paper to overcome the shortcomings of interaction method. Second, a virtual mass distribution function (VMDF) is proposed for calculating coarse particle volume fraction. Third, a weighted function method (WFM) relating the particle size is given for the interpolation between the Eulerian and Lagrangian field for coarse particles. Fourth, the optimized method is applicable to both the fine and coarse particle in two-phase flow.[37]

III. NUMERICAL VALIDATION

An experiment case is given, and the experimental apparatus includes four parts: vertical pipe, circulating water system, control system, and image acquisition device (as shown in Fig. 3). The vertical pipe has an inner diameter of 50 mm and a height of 3 m. An electromagnetic flowmeter is installed in the middle of the pipe to measure the flow rate. 700 particles of diameter 6 mm (600) and 13 mm (100) are mixed and placed at the bottom of the pipe initially. The initial height of the mixed particles is about 150 mm. The pump is turned on to form a transportation water flow. The particles are glass beads with a density of 2600 kg/m^3. The water density and viscosity are 1000 kg/m^3 and 0.001 Pa · s, respectively. The particle movement is imaged as the flow rate increasing.

As the flow rate increases slowly from 0 m^3/h, the mixed particles remain static initially. When the flow rate reaches 0.12 m^3/h, several particles start to move on the upper part of the particle bed. When the flow rate reaches 0.28 m^3/h, some of the particles of diameter 6 mm have moved to the upper part of the bed. Then, the particles of diameter 6 mm are completely separated from the particle bed with obvious segregation when the flow rate reaches 0.35 m^3/h. The particles of diameter 6 mm are in a fluidized state, while the particles of diameter 13 mm have not reached the fluidized state. When the flow

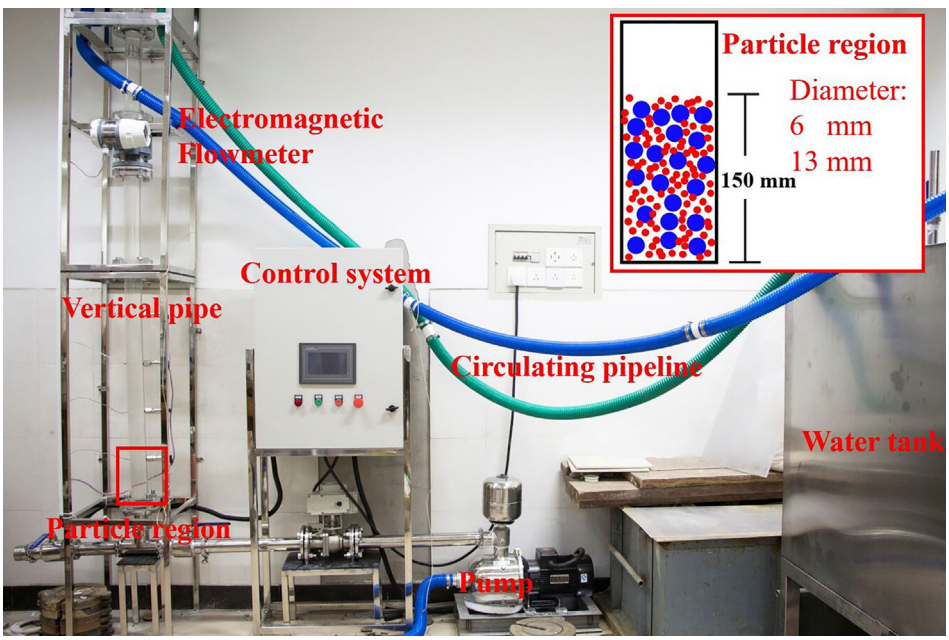

FIG. 3. The experimental apparatus, which includes four parts: vertical pipe, circulating water system, control system, and image acquisition device. The initial height of the mixed particles (6 and 13 mm) is about 150 mm.

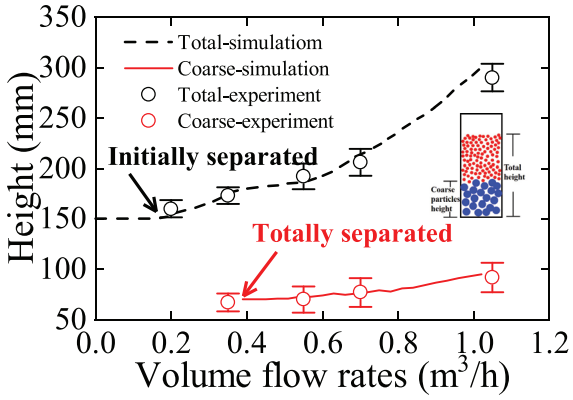

FIG. 4. Comparison between the simulation results and the experimental results of the particle height at different volume flow rates. "Total" means the total height of the particles. "Coarse" means the height of the particles with a diameter of 13 mm.

rate reaches 0.7 m^3/h, the expansion height of the particle bed increases and the particles of diameter 13 mm reach the fluidized state. The simulation results and the experimental results are given in Fig. 4, where the total height and the coarse particles (13 mm) height are shown. The comparison between the simulation results and the experimental results shows that the method is capable to capture the main flow behaviors of hydraulic lifting.

IV. NUMERICAL SETUP

It is difficult to handle hydraulic lifting equipment directly and to perform the expensive tests due to the specificity and complexity of the deep-sea environment. In the hydraulic lifting process, the system is affected not only by the mining vessel and ship but also by the forces of gravity, pressure, oceanic hydrodynamics, and so on. Therefore, the transportation of particles in the vertical pipeline of the hydraulic lifting system is simulated to explore the characteristics and effects of the internal flow in this section. In the hydraulic lifting process, the concentration of particles usually exceeds 10^{-3} vol.%. The vol.% means the percentage of the particle volume in the total volume of the two phases. As a result, the four-way coupling,[52] where both the fluid–solid interaction and particle–particle interaction are considered, is used.

Manganese nodules on the deep seabed have complex forms and broad particle size distributions. Some of the nodules are larger than 50 mm, which will result in high power consumption and even blockage. Consequently, the nodules are broken into smaller particles (about 5–30 mm) before transporting into the vertical pipe, but not excessively broken, as too small nodules may be discharged as slude.[4,53] We assume that the size of the particles corresponds to a normal distribution, which is described by the expectation (d) and the variance (σ) of the normal distribution. According to the literature research[4,31,54–56] and project design in "Chinese Academy of Sciences Strategic Leading Science and Technology Project," the particle inlet volume fraction (or concentration) α_{p0} is 0.06–0.15 vol.%, and the water inlet velocity u_0 is 1–5 m/s. The particle density is about 1500–2500 kg/m^3. The Young's modulus E and Poisson's ratio ν of the particles are 1.0×10^{10} Pa and 0.11. The density of water is 1000 kg/m^3, and water viscosity is 0.001 Pa · s. The unit of the particle concentration in this paper is vol.%.

Fluid phase equations (5) and (6) are discretized in a three-dimensional Eulerian grid with the finite volume method (FVM). The second-order Gauss–Green integral method is used to discretize the gradient term, the second-order upwind scheme is used for the divergence term, and the Laplacian term is treated with Gauss–Green integral method with non-orthogonal correction. For the time discretization, a second-order scheme is adopted. Fluid velocity and pressure are decoupled using the pressure implicit with splitting of operators (PISO) algorithm, and then, the corresponding linear algebraic systems can be obtained for velocity components and pressure correction values. The discretized algebraic equations of the pressure Poisson equation and momentum equation are solved by the algebraic multigrid method and smother solver in open-source code OpenFOAM.[46] The discretized algebraic equations of the diffusion equations added in the VMDF method are solved by preconditioned conjugate gradient (PCG) method. The time step for the fluid phase is determined by setting the Courant number less than 0.5. Particle motion is solved within the Lagrangian framework, and Eqs. (1) and (2) are integrated using the implicit Euler scheme. The leapfrog integration algorithm is used to calculate the velocity of the particle due to the particle collisions.[57] In general, the time step for the particle simulation should be much smaller than the fluid time step. In this paper, the time step for the particle simulation is same to that of fluid phase because the barycentric tracking method is used in the particle tracking, where the particle tracking is divided into many steps by the intersection of the particle trajectory and the cell face.[58] The related fields are decomposed into multiple blocks using the decomposePar tool, and each separate block in the decomposed fields is run on the cluster of the BeiJing High Performance Computing (HPC) with 64 AMD EPYC 7452 CPU 2.35 GHz and 256 GB RAM using OpenMPI (an implementation of the standard message passing interface).

A vertical pipe with an internal diameter of $D = 200$ mm and a length of $H = 6$ m as indicated in Fig. 5 is defined in the present document. Three cylinder regions with the same diameter with the vertical pipe are set to store the simulation data, which are located at $z = 0.2$ m, $z = 3.0$ m, and $z = 5.8$ m. The mixture of the particles and water enters the vertical pipe from the bottom and exits from the top. An O-grid is established for the computational domain using ANSYS ICEM. After the cell independence test, the number of cells is 240 000 with 21, 41, and 601 nodes in the radial, hoop, and axial direction. The ratio of the average particle diameter to the cell size is about 1.5. The pipe wall is set to be zero value for the water velocity and zero gradient for the relative motion pressure P_{rgh}. The outlet face (upper z-direction) is set to be zero value for the relative motion pressure and zero gradient for the water velocity, and the inlet face (lower z-direction) is set to a fixed velocity for the water and zero gradient for the relative motion pressure. The velocity of the particles at the inlet is defined as zero. The particle volume fraction or concentration at the inlet, which is used to indicate the number of particles entering the pipe in engineering, needs to be modified to the particle numbers per second:

$$N_p = \frac{\frac{\pi}{4} D^2 u_0 \alpha_{p0} \int_{d_{min}}^{d_{max}} f(x)\mathrm{d}x}{\int_{d_{min}}^{d_{max}} f(x) \frac{\pi}{6} x^3 \mathrm{d}x}, \tag{15}$$

where N_p is the particle numbers per second, d_{min} and d_{max} are the minimum and maximum particle diameter, respectively, and $f(x)$ is

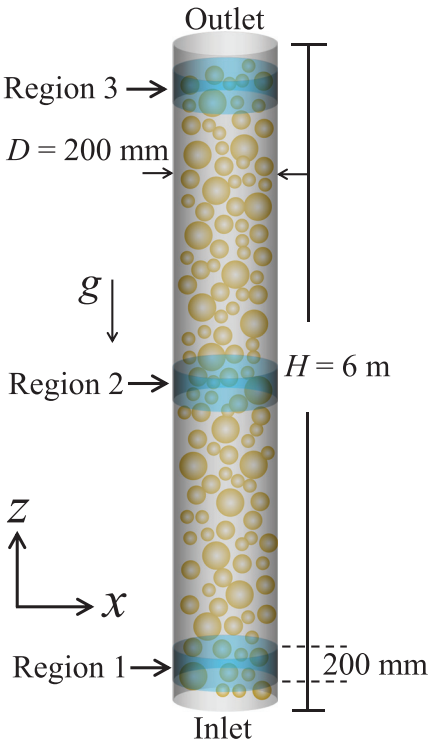

FIG. 5. The vertical pipe with an inner diameter of 200 mm and a length of 6 m. The mixture of the particles and water enters the pipe from the bottom.

the probability density function of particle size distribution, and is expressed as

$$f(x) = \frac{1}{2\pi\sigma}\exp\left(-\frac{(x-d)^2}{2\sigma^2}\right), \tag{16}$$

where d is the average particle diameter. At the initial condition, the vertical pipe is full of water with zero value for the velocity, particle concentration, and relative motion pressure.

In the actual hydraulic lifting process, the length of the vertical pipe is larger than 1000 m. It is impractical to model with a 1:1 ratio given the simulation consumption. In fact, the particles are mixed with water during an initial period after entering the vertical pipe and will tend to be stable after being completely mixed uniformly. Hence, only a certain length of the pipe is required to make the particle transportation reach a steady state. Figure 6 gives the particle concentration, particle vertical velocity, and slip velocity at different locations of the vertical pipe when the transportation reaches a stable condition with a pipe length of 20 m. The slip velocity $\mathbf{u}_s$ in this paper is defined as $\mathbf{u}_s = \mathbf{u} - \mathbf{v}$. The parameters are given in Table I. It is shown that the particle transportation becomes stable at about $z > 3$ m. As a result, the pipe length in this paper is set as 6 m for reducing the computation cost.

V. RESULTS AND DISCUSSION

A. Internal flow field analysis

Velocity and particle concentration are two main parameters for investigating the solid–liquid two-phase flow. Furthermore, slip

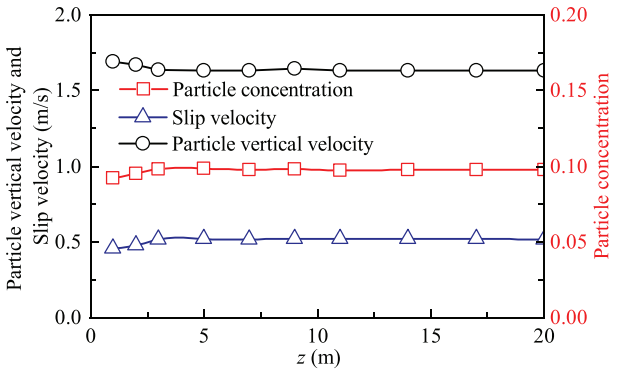

FIG. 6. Comparison of particle concentration, particle vertical velocity and slip velocity at different locations of the vertical pipe when the transportation reaches a stable condition with a pipe length of 20 m.

velocity is another important factor for coarse particles due to poor following performance of the coarse particles. Based on the numerical simulation results, the flow field information in the vertical pipe under different parameters is obtained. First, a standard case is taken as an example to provide insight into the coarse particles transportation in the hydraulic lifting process. All parameters used in the standard case are identical to Table I, with the exception of the length of the pipe, which is set as 6 m. Figure 7 presents twelve images at different times and regions during the lifting process. The horizontal direction is the z axis, and the vertical direction is the y axis. In order to capture different flow behaviors in the length direction, we selected two sections, 0–2 m and 3–5 m in the z direction. The color of these particles denotes their sizes. The time-varying curve of the volume-averaged

TABLE I. Parameters used in the numerical simulation of the hydraulic lifting of coarse particles with different pipe lengths.

Parameters	Values
Geometry of the vertical pipe	
Diameter	200 mm
Length	20 m
Particle properties	
Density ρ_p	2000 kg/m^3
Average diameter d	15 mm
Variance σ	2 mm
Inlet concentration α_{p0}	0.08 vol.%
Young's modulus E	1.0×10^{10} Pa
Poisson's ratio ν	0.11
Coefficient of restitution for particle–particle/wall α/α_w	0.02/0.01
Coefficient of friction for particle–particle/wall μ/μ_w	0.10/0.09
Water properties	
Density ρ_f	1000 kg/m^3
Viscosity μ_f	1.0×10^{-3} Pa · s
Inlet velocity u_0	2 m/s

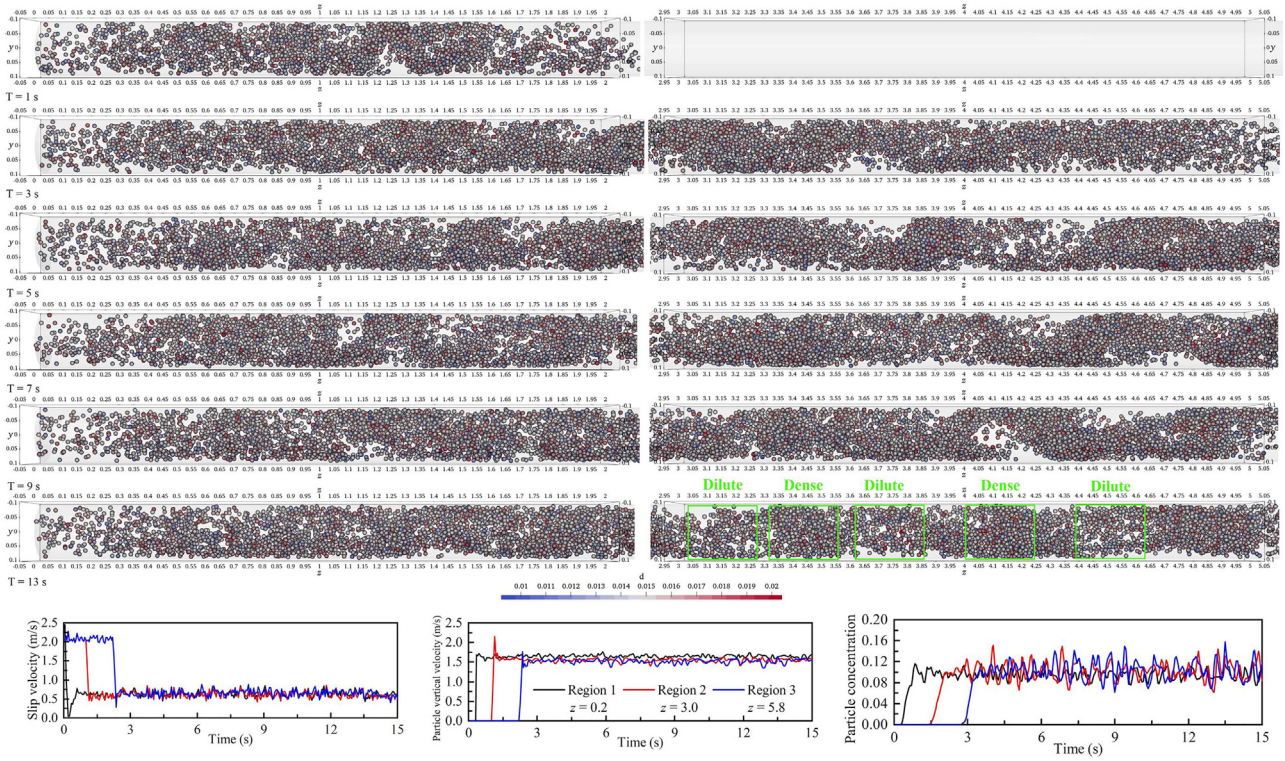

FIG. 7. The particle distribution in the vertical pipe in hydraulic lifting at the time of 1, 3, 5, 7, 9, and 13 s. The color of these particles denotes their sizes.

slip velocity, particle vertical velocity, and the particle concentration at the three regions (Fig. 5) are also illustrated in Fig. 7. The volume-averaged value is defined as

$$\langle u_s \rangle = \left| \frac{1}{N_c} \sum_{i=1}^{N_c} \mathbf{u}_{s,i} \right|; \quad \langle \alpha_p \rangle = \frac{1}{N_c} \sum_{i=1}^{N_c} \alpha_{p,i}; \quad \langle v_p \rangle = \frac{1}{N_c} \sum_{i=1}^{N_c} v_{z,i}, \tag{17}$$

where $\langle u_s \rangle$, $\langle \alpha_p \rangle$, and $\langle v_p \rangle$ are the volume-averaged slip velocity, particle concentration, and particle vertical velocity, respectively, N_c is the total cell number in the selected domain (regions 1, 2, and 3), and $\mathbf{u}_{s,i}$, $\alpha_{p,i}$, and $v_{z,i}$ are the slip velocity, particle concentration, and particle vertical velocity (z-direction) in cell i, respectively. At the beginning of the hydraulic lifting, particles mix with the water and go upwards. The particle concentration at the top of the particle group (see T = 1 s in Fig. 7) is lower than the middle part. It may result from particle segregation that fine particles move faster than the coarse particles. It can be clearly seen that the particle concentration inside the pipe is significantly greater than that at the inlet of the pipe. This phenomenon is called particle retention, which is very obvious in the transportation of coarse particles. The particle retention will be discussed in detail in Sec. V B. The vertical pipe is filled with particles at the time of approximately 4 s. Then, the two-phase flow in the vertical pipe has reached a stable state and the overall particle numbers in the pipe are almost unchanged. For example, the slip velocity, particle vertical velocity, and particle concentration in region 3 (Fig. 7) become stable with time after the time of approximately 4 s. In this paper, the stable state is defined as that the time-averaged value is unchanged over time. However, the time series of value such as the particle concentration is pulsating. The pulsation process appears to be explained by three factors. First, the turbulence irregularity of the water movement in the vertical pipe makes the velocity of the water pulsating. Hence, the drag force on the particle is also pulsating. Second, the pulsation results from the dynamic change of the force on the particles due to the change of the particle concentration. Third, collisions between particles or particles and the wall are instantaneous, resulting in instantaneous changes in the total forces of the particles.

According to the time-varying curve trend illustrated in Fig. 7 and combined with the numerical results of the particle distribution, the particle transportation process in the vertical pipe can be roughly divided into three stages: single phase flow stage (stage I), mixing stage (stage II), and stable transportation stage (stage III). Figure 8 shows

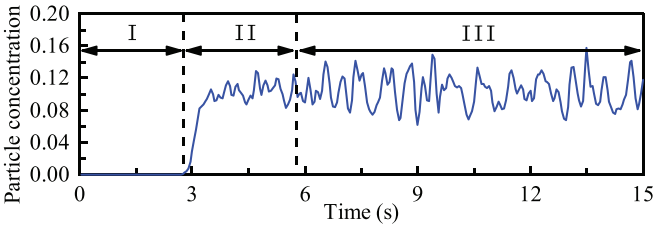

FIG. 8. Volume-averaged particle concentration in the vertical pipe (region 3). The curve can be divided into three stages over time: single phase flow stage (stage I); mixing stage (stage II); stable transportation stage (stage III).

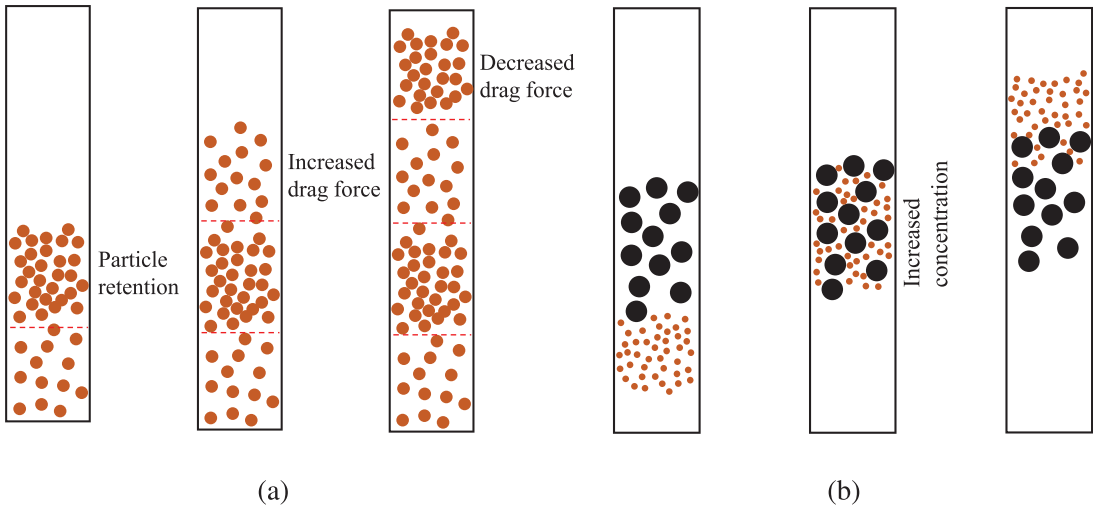

FIG. 9. Different stages of development for the dilute-dense flow pattern of the solid–liquid two-phase flow with coarse particles: (a) particle retention and (b) particle size segregation.

the three stages. (I) Stage I: Single phase flow stage. At the initial condition, the vertical pipe is free of particles. The particle concentration in the pipe is zero until the particles reach the selected region. Hence, this stage is called single phase flow stage. (II) Stage II: Mixing stage. The mixing stage means the initial mixing between the particles and water. Once the particles reach the selected region, the appearance of the particles increases the particle concentration from zero to a certain value, which results in the changes in the water velocity and the force on the particles. As such, certain instability occurs, such as a sudden increase or decrease in particle velocity. (III) Stage III: Stable transportation stage. The hydraulic lifting tends to be stable with time-averaged value unchanged with time. At the stable transportation stage, the particles show a dense-dilute flow pattern, as shown in the T = 13 s in Fig. 7. According the experiments of Zhang *et al.*,[37] the dilute-dense flow pattern is obvious in the two-phase flow with coarse particles. Figure 9 provides a brief illustration of the particle distribution in the vertical pipe to show the underlying mechanisms of the dense-dilute flow pattern. First, due to the density difference between the coarse particles and the water, velocity of the particles is lower than the carrying water, which makes the particle retention in the pipe [Fig. 9(a)]. The particle retention in the pipe increases the local particle concentration and the water velocity because the flow area of water is reduced. Then, the drag forces on the particles increase and the particles move upward faster. As the particles move upwards, the gaps between the particles become larger. Then, the flow area of the water, and the water velocity decreases, which results in the decrease in the drag force. The particle vertical velocity and particle local concentration correspondingly decrease. Second, the particle size segregation can also lead to the dilute-dense flow pattern, as shown in Fig. 9(b). During the hydraulic lifting, the fine particles will move around the coarse particles. To show the particle size segregation, the concentration of the particles of sizes of 5–10 mm in the particle group is studied. Figure 10 gives the distribution of the ratio of the concentration of fine particles to the total particle concentration along the central axis of the pipe at times of 12and 13 s, which is in the stage III. The position of $z/H = 0$ indicates the bottom of the pipe, and the position of $z/H = 1.0$ indicates the pipe outlet. The ratio of fine particle concentration to total particle concentration at times of 12 and 13 s shows an almost inverse distribution. This means that the fine particles move upwards in the pipe over the coarse particles, which results in the change of the total particle concentration and the particle forces. Hence, the particle group shows a dilute-dense flow pattern.

Figure 11 gives radial distribution of the particle concentration and the particle vertical velocity at the middle of the vertical pipe ($z = 3$ m). The position of $x/R = 0$ indicates the center of the pipe, and the position of $x/R = \pm 1.0$ indicates the pipe wall. The red dot line in Fig. 11 is the time-averaged value. At the time of 12 s, the local particle concentration in the range of $x/R < 0$ is larger than that of $x/R > 0$. However, the local particle concentration in the range of $x/R < 0$ is smaller than that of $x/R > 0$ by the time of 15 s. The time-averaged value of the local particle concentration and the vertical particle velocity in the radial direction is almost the same.

Figure 12 is the contour of particle concentration and water velocity at longitudinal section of the vertical pipe (section $y = 0$). In order to make the contour clear, the display scale of the x axis and the z axis has been modified from 1:1 to 1:2. From left to right, the contours are the instantaneous value at the time of 1 s, the instantaneous

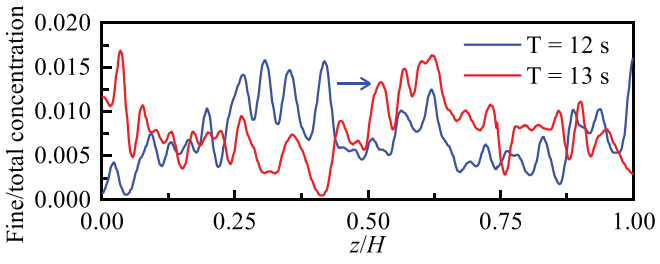

FIG. 10. Distribution of the ratio of the concentration of fine particles to the total particle concentration along the central axis of the pipe at times of 12 and 13 s.

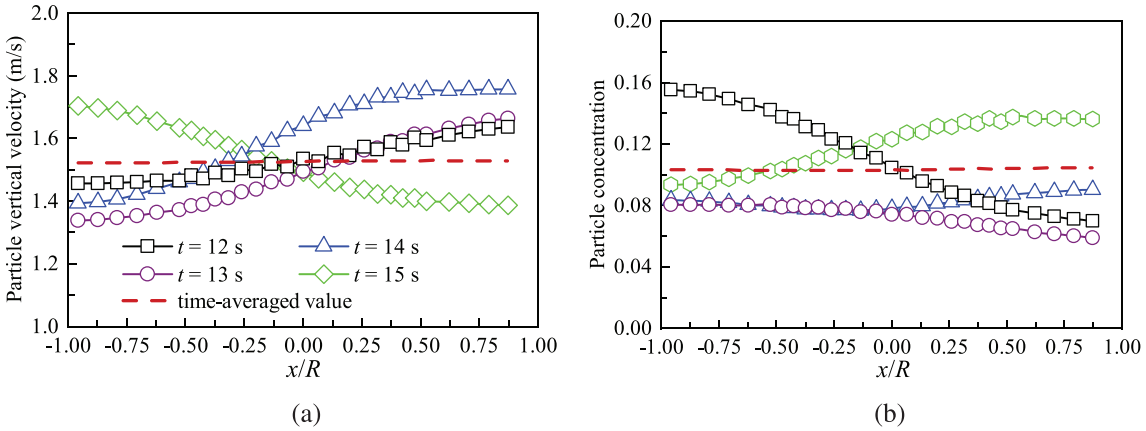

FIG. 11. The radial distribution of the (a) particle vertical velocity and (b) particle concentration at the middle of the vertical pipe ($z = 3$ m) in hydraulic lifting. The red dot line is the time-averaged value.

value at the time of 11 s, and the time-averaged value. The particles height is about 2.2 m at the time of 1 s, and there are no particles in the interval of $z = 2.2$ m–6 m of the pipe. The particle concentration at the top and bottom of the particle group is significantly smaller than the middle area, which is similar to Fig. 7. The particles in the middle area of the particle group are concentrated on the right side of the pipe (x axis positive direction) at the time of 1 s. This is because the particles are in a dilute-dense state during the transportation process. At the time of 11 s, the vertical pipe is full of particles and the transportation reaches a steady state, which clearly shows a dilute-dense flow pattern. From the bottom to the top of the pipe, the particle concentration areas alternately appear along the z-direction of the pipe. The appearance of a concentrated area of particle is detrimental to the hydraulic lifting process. The interaction between particles and the interaction between particles and the pipe wall will increase, which cause more energy consumption and increase flow resistance. The water velocity is exactly the same in the area of $z = 2.2$–6 m in Fig. 12(b). However, in the area of the mixture of particles and water, the motion of water is disturbed due to the interaction between water and particles, which cause a maximum water velocity of 3 m/s. Compared with the instantaneous value, the time-averaged value of the particle concentration and water velocity is uniformly distributed in the pipe. It means that the particle transportation in the pipe is stable. The instantaneous value can better reflect the true transportation process.

B. Analysis of retention of particles

It is found that the local particle concentration in the vertical pipe is greater than the inlet particle concentration at the bottom of the pipe (Fig. 7). For the standard case, the particle concentration at the inlet is 0.08, while the time-averaged local particle concentrations in regions 1, 2, and 3 are approximately 0.093, 0.102, and 0.104. This phenomenon is called a particle retention in the hydraulic lifting.[59] The reason for particle retention is that when particles move along the water, the particles cannot follow the water entirely due to the greater density of particles than water. It produces a velocity slip between the particles and the water, which will make the particles accumulate in the vertical pipe, and then produce the particle retention. The particle retention in hydraulic lifting is a very important cause of pipe blockage.[34] To further analyze the particle retention process in hydraulic lifting, Fig. 13 shows the change of the local particle concentration under different parameters, such as the inlet water velocity, inlet particle concentration, particle density, and so on. The data of the local particle concentration are extracted from the region 2 with time-averaged value of the volume-averaged results. From the time-varying curve of the particle concentration in Fig. 8, the hydraulic lifting process tends to be stable with time. Hence, the data in the stable transportation stage (stage III) of the particle transportation are used because of the short duration of the stage I and stage II. All parameters have the same values as in Table I except for the current parameters in the figure.

As shown in Fig. 13(a), the local particle concentration decreases from 0.15 to 0.10 as the water inlet velocity increases from 1 to 5 m/s with particle inlet concentration of 0.10. The local particle concentration is always larger than the inlet particle concentration over the range of water inlet velocity $u_0 = 1$–5 m/s. The local particle concentration decreases faster in the u_0 interval from 1 to 2.5 m/s. However, when the water inlet velocity is further increasing, the decrease in local particle concentration slows down and gradually tends to be a constant value. That is, the particle retention phenomenon alleviates with the increase in the water inlet velocity, and almost disappears at a higher water inlet velocity. It should be noted that, regardless of the water inlet velocity, the lower limit of the particle local concentration is the inlet particle concentration. This is because the particles depend upon the traction of the water to rise, and the driving energy of the movement of the particles comes from the water. Therefore, the particle velocity is less than or equal to the water velocity. Although at some transient moments, the particle vertical velocity is greater than the water velocity due to particle collisions. The overall velocity of particle movement after time averaging is still less than or equal to the water velocity. In other words, the particles will stagnate or move only at the same velocity as the water by moving upward in the vertical pipe. The particle retention is an important factor for particle clogging occurrence in the vertical pipe. High-speed internal flow provides the comparatively large axial force, so properly increasing the water inlet velocity can alleviate this phenomenon. However, higher water inlet velocity requires more energy input and correspondingly higher

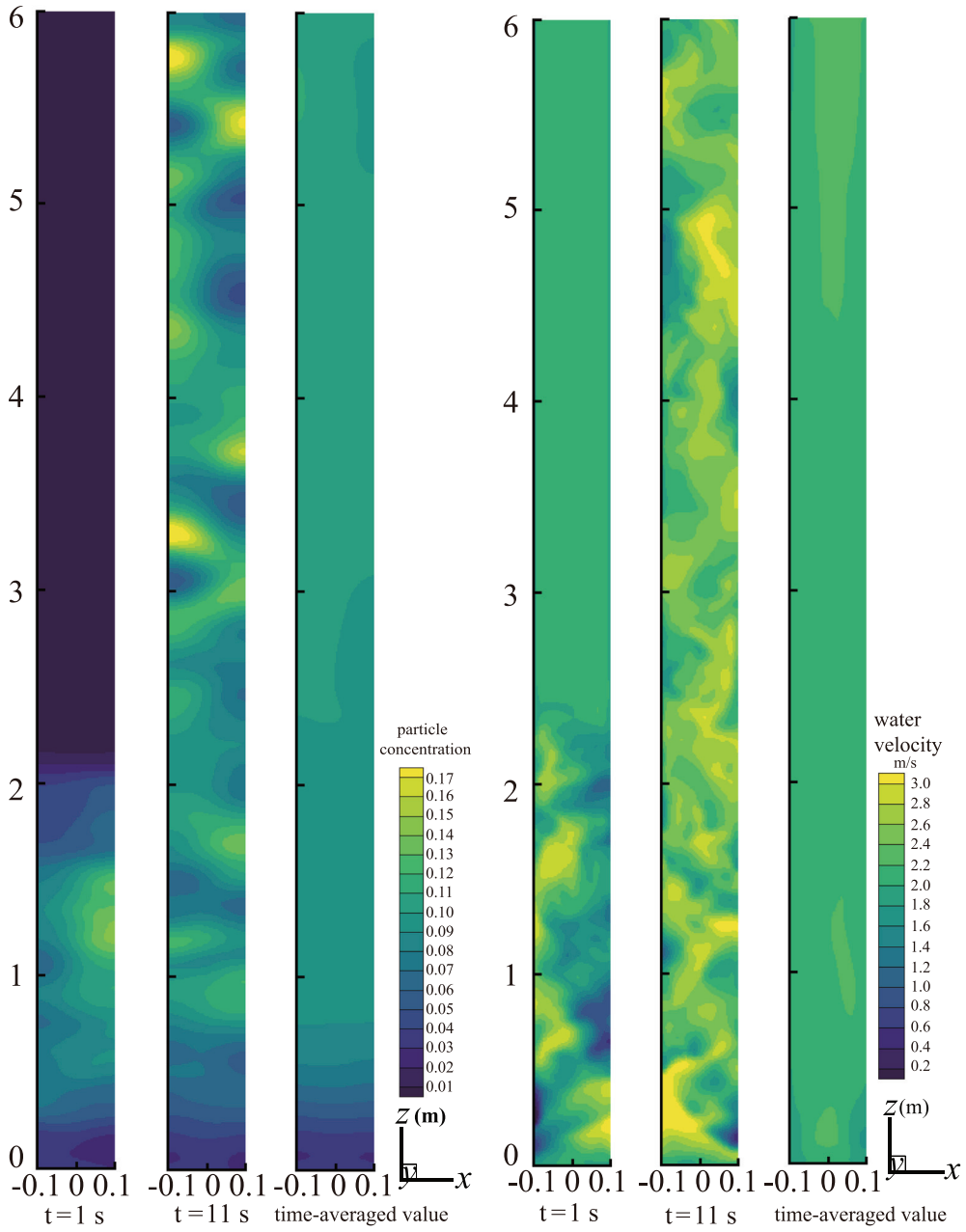

FIG. 12. The contour of (a) particle concentration and (b) water velocity at longitudinal section of the vertical pipe ($y = 0$). The contours in (a) and (b) are the instantaneous value at the time of 1 s, the instantaneous value at the time of 11 s, and the time-averaged value from left to right. The scale ratio is $x : z = 1 : 2$ (a) and (b), respectively.

economic cost, which is also a factor to be considered. It is found that at the water inlet velocity of about 2–3 m/s, the turning point of the particle local concentration curve appears, which may be chosen as the most economical water inlet velocity. There are many kinds of particle materials in hydraulic lifting, including polymetallic nodules and sulfides. The main difference lies in the density. Therefore, five different densities of particles, namely, 1500, 1750, 2000, 2250, and 2500 kg/m^3, are considered and discussed in this section. Figure 13(c) shows the variation of particle local concentration in region 2 for different particle densities. The particle density has a great influence on the particle local concentration in the vertical pipe. As the density of particle increases, the local concentration of particle gradually

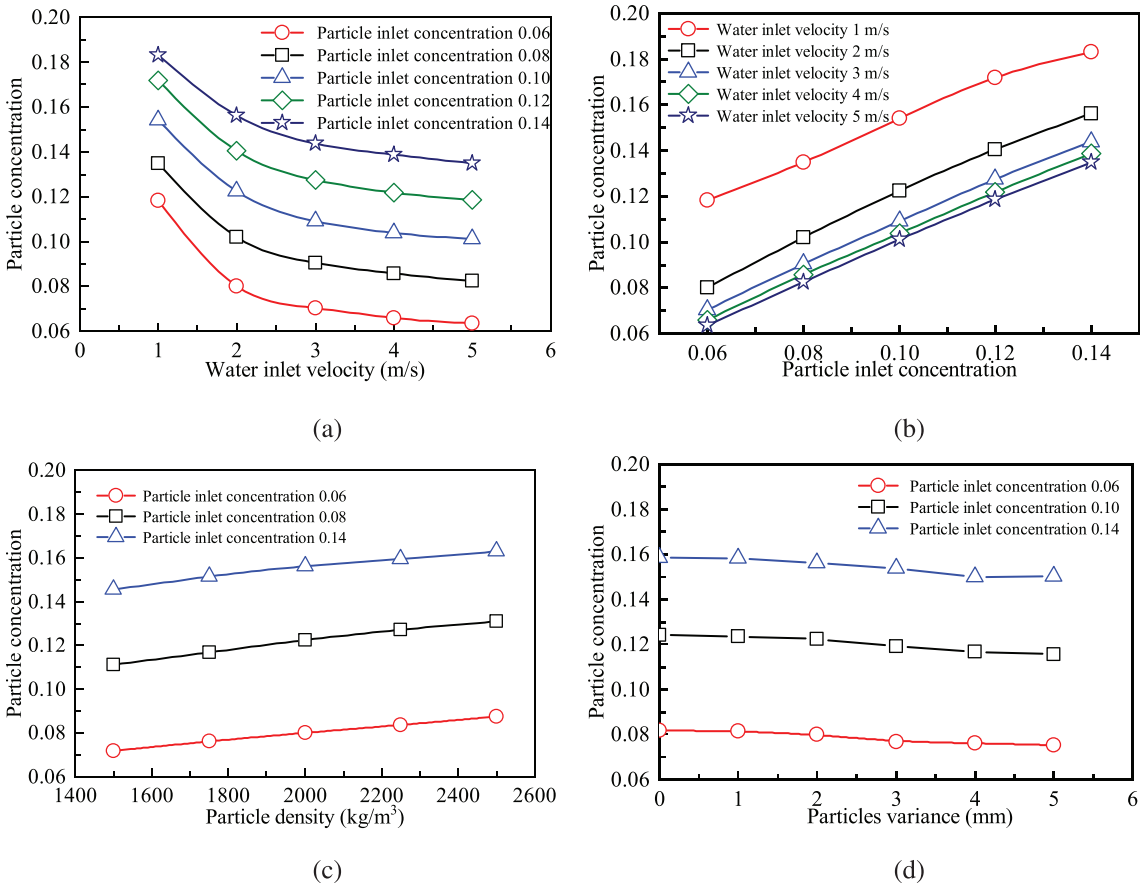

FIG. 13. Effect of (a) water inlet velocity, (b) particle inlet concentration, (c) particle density, and (d) particles variance on the local particle concentration. The data are extracted from the region 2 with time-averaged value of the volume-averaged results.

increases. The gravitational force of the particles increases due to the increase in the particle density, while the water drag forces on the particles remain unchanged when other conditions remain the same. In this way, the overall ascending force on the particles decreases, which results in a decrease in the velocity of the particles and a deterioration in the follow capability of the particles. The particles variance σ indicates the particle size distribution. The higher the variance, the more scattered the particle size distribution. When the variance is 0, it means that the particle sizes are uniformly distributed. The variance of particle size is not influential to local particle concentration.

C. Analysis of hydraulic lifting performance

The hydraulic lifting process is affected by several factors (ρ_f, μ_f, d, ρ_p, D, g, u_0, α_{p0}). The vertical velocity of the particles in the vertical pipe $v_{p,z}$ during the stable transportation stage (stage III) in Fig. 6 can be written as

$$v_{p,z} = f\left(\rho_f, \mu_f, d, \rho_d, D, g, u_0, \alpha_{p0}\right). \tag{18}$$

Choosing ρ_f, u_0, and d as unit system, the dimensionless expression of Eq. (18) can be written as:[60]

$$\frac{v_{p,z}}{u_0} = f\left(\frac{\rho_f u_0 d}{\mu_f}, \frac{\rho_p}{\rho_f}, \frac{d}{D}, \sqrt{\frac{gd}{u_0^2}}, \alpha_{p0}\right), \tag{19}$$

where $\frac{v_{p,z}}{u_0}$ is the ratio of the vertical velocity of particles in the pipe to the water inlet velocity; $\frac{\rho_f u_0 d}{\mu_f}$ is the transport Reynolds number, which characterizes the ratio of inertial force to viscous force; $\frac{\rho_p}{\rho_f}$ is the density ratio; $\frac{d}{D}$ is the relative particle diameter; and $\sqrt{\frac{gd}{u_0^2}}$ is the Froude number, which represents the ratio of inertia force to gravity.

First, the relationship between the vertical velocity of particles and dimensionless parameters in Eq. (19) is analyzed. The hydraulic lifting process is similar to the physical process of particles settling in water. The analogous analysis can be made by the process of particle settling. Single particle is subject to gravity, buoyancy, and resistance when settling in static water, which will undergo the transition process from accelerated to uniform settling velocity. The terminal velocity of a single particle settling in still water is calculated as[60]

$$v_t = \sqrt{\frac{4(\rho_p - \rho_f)gd}{3\rho_f C_d}} = \sqrt{\frac{\rho_p}{\rho_f} - 1}\sqrt{\frac{4gd}{3C_d}}. \tag{20}$$

The relationship between the relative particle vertical velocity and density ratio is assumed to be $\frac{v_{p,z}}{u_0} \sim \sqrt{\frac{\rho_p}{\rho_f} - 1}$, and the relationship with the Froude number is $\frac{v_{p,z}}{u_0} \sim \frac{\sqrt{gd}}{u_0}$. Xia *et al.*[59] investigated the minimum fluidization velocity of particles in a fixed bed, which requires the introduction of a $(1 - \frac{d}{D})^2$ correction when a circular tube wall surface is present. Therefore, the relationship between the relative particle vertical velocity and the relative particle diameter is assumed to be $\frac{v_{p,z}}{u_0} \sim (1 - \frac{d}{D})^b$, where b is a constant. Van Wijk *et al.*[35] derived a model for the disturbance settling terminal velocity based on the fluid resistance at the particle boundary and gave experimental verification. Inspired by the work of Van Wijk *et al.*,[35] it is assumed that the relative particle vertical velocity is related to the particle inlet concentration as $\frac{v_{p,z}}{u_0} \sim (1 - \alpha_{p0})^e$, where e is a constant. Since the values of $\frac{v_{p,z}}{u_0}$ range from 0 to 1, Eq. (19) is rewritten as

$$\frac{v_{p,z}}{u_0} = 1 - a\sqrt{\frac{\rho_p}{\rho_f} - 1}\left(1 - \frac{d}{D}\right)^b \left(\frac{\sqrt{gd}}{u_0}\right)^c (1 - \alpha_{p0})^e, \quad (21)$$

where a, b, c, and e are constants. Subsequently, a multiple regression analysis is performed on expression (21) based on the numerical simulation results. The fitting yields $a = 4.4$, $b = 7.8$, $c = 1$, and $e = 7.9$. The fitted correlation coefficient $R^2 = 0.95$. Then, the specific form of the expression (21) is

$$\frac{v_{p,z}}{u_0} = 1 - 4.4\sqrt{\frac{\rho_p}{\rho_f} - 1}\left(1 - \frac{d}{D}\right)^{7.8} \left(\frac{\sqrt{gd}}{u_0}\right)(1 - \alpha_{p0})^{7.9}. \quad (22)$$

When the upward motion velocity of the particle group is below zero, it means that the particle group cannot move up continuously under such conditions. Assuming Eq. (22) equal to zero gives

$$u_{0,cr} = 4.4(1 - \alpha_{p0})^{7.9}\left(1 - \frac{d}{D}\right)^{7.8} \sqrt{\frac{(\rho_p - \rho_f)gd}{\rho_f}}, \quad (23)$$

where $u_{0,cr}$ is the critical hydraulic lifting velocity. Only when the water inlet velocity is greater than this critical velocity, the particles can continuously move upward. There is a clear physical meaning for Eq. (23). The last term on the right-hand side of Eq. (23) is similar to the terminal settling velocity of a single particle in static water. The second and third terms on the right-hand side are the particle concentration correction as well as the pipe wall correction. However, the actual particles are not standard spherical. For safety considerations, a safety factor S needs to be multiplied. As such, the critical velocity is derived by the following form:

$$u_{0,cr} = 4.4S(1 - \alpha_{p0})^{7.9}\left(1 - \frac{d}{D}\right)^{7.8} \sqrt{\frac{(\rho_p - \rho_f)gd}{\rho_f}}. \quad (24)$$

The safety factor can be set as 2.3.[61] The relationship between $\frac{u_{0,cr}}{\sqrt{(s-1)gd}}$ and particle inlet concentration α_{p0} based on formula (24) and the experimental results from Jin *et al.*[62] is shown in Fig. 14, where $s = \rho_p/\rho_f$ is the density ratio. It shows a good comparison between the calculated and experimental results, which proves the accuracy of the formula (24). Formula (24) can be used to predict the critical velocity in the vertical pipe during hydraulic lifting.

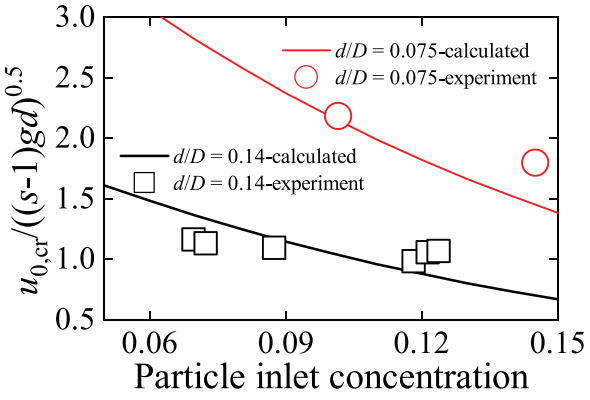

FIG. 14. Comparison between the predicted results and the experimental results.

Assuming that all parameters are the same as those in Table I, the variation of the critical hydraulic lifting velocity $u_{0,cr}$ and the amount of particles lifted Q with the inlet particle concentration α_{p0} is shown in Fig. 15. The amount of particles lifted is expressed as

$$Q = \frac{\pi}{4} D^2 u_0 \alpha_{p0} \rho_p. \quad (25)$$

The most important parameters in the design of the hydraulic lifting are the water inlet velocity and the particle inlet concentration. The critical hydraulic lifting velocity decreases with the increase in the particle inlet concentration, but the amount of particles lifted tends to increase and then decrease with the increase in α_{p0}. Based on the aforementioned results, to consider the economy and stable operation, the particle inlet concentration and water inlet velocity should be controlled within an appropriate range. It is recommended that the particle inlet concentration is around 0.01, and the water inlet velocity is around 2–3 m/s.

Second, the hydraulic gradient in the hydraulic lifting is analyzed. Xia *et al.*[59] proposed an equation to calculate the hydraulic gradient of the hydraulic lifting, which consists of three parts: hydraulic gradient due to the flow of water, i_f, hydraulic gradient from the presence of the particles, i_p, and the hydraulic gradient associated with particle collisions, i_c. The total hydraulic gradient i_t of the mixture (water and

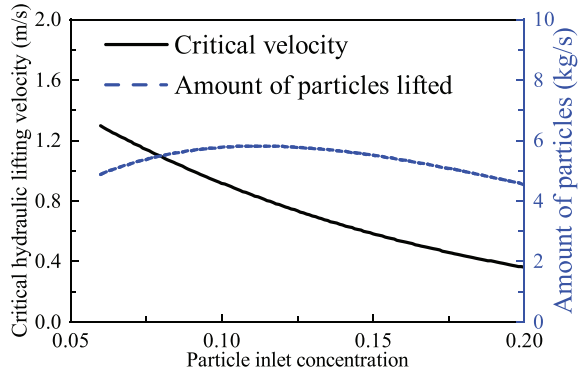

FIG. 15. The variation of the critical hydraulic lifting velocity $u_{0,cr}$ and the amount of particles lifted Q with the inlet particle concentration α_{p0}.

particles) can be expressed as $i_t = i_f + i_p + i_c$. The hydraulic gradient produced by the flow of water is calculated by $i_f = \lambda u_0^2/(2gD)$, where λ is coefficient of friction, which can be defined by Moody diagram[63] based on Reynolds number and relative roughness of the vertical pipe. An additional static pressure drop will occur for the two-phase flow due to the higher density of the particles to that of water. As a result, the hydraulic gradient from the presence of the particles can be expressed as $i_p = \alpha_p(\rho_p/\rho_f - 1)$. It is recommended by Xia *et al.*[59] that the effect of the particle collisions cannot be neglected in two-phase flows with particle concentration greater than 0.04. The hydraulic gradient associated with particle collisions is derived from the decrease in potential energy of the two-phase.[59] In this paper, the computational model above is simplified by considering the sum of i_f and i_c as the hydraulic gradient of mixture and assuming that it can be expressed as

$$i_m = C_P \frac{u_0^2}{2gD}, \tag{26}$$

where i_m is the hydraulic gradient of the mixture and C_P is the coefficient of friction for the mixture. The pressure drop of the mixture in a unit length of the vertical pipe during the hydraulic lifting process can be written as[64]

$$\frac{\Delta P}{H} = \alpha_p(\rho_p - \rho_f)g + \frac{\tau_m}{D}, \tag{27}$$

where H is the length of the selection pipe section and τ_m is the frictional resistance of the pipe wall to the solid–liquid mixture. Then, τ_m is expressed as

$$\tau_m = \left[\frac{\Delta P}{H} - \alpha_p(\rho_p - \rho_f)g\right]D. \tag{28}$$

The coefficient of friction for the mixture C_P in this paper is defined by

$$C_P = \frac{\tau_m}{\frac{1}{2}\rho_f u_0^2}. \tag{29}$$

The change of the coefficient of friction for the mixture (C_P) under different parameters, such as the water inlet velocity, particle inlet concentration, particle density, and so on, is shown in Fig. 16. Similar to Fig. 13, the data are extracted from the region 2 with time-averaged

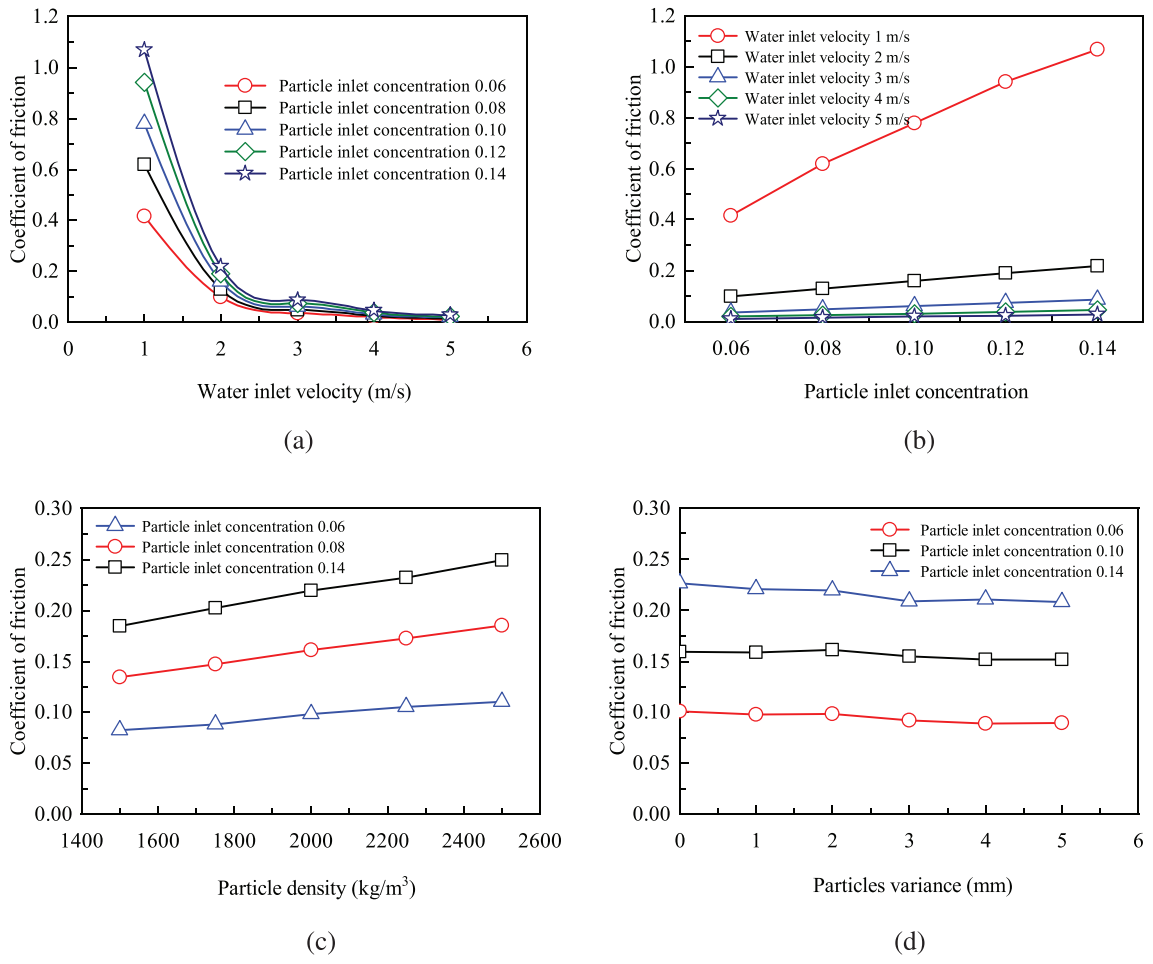

FIG. 16. Effect of (a) water inlet velocity, (b) particle inlet concentration, (c) particle density, and (d) particles variance on the coefficient of friction for the mixture. The data are extracted from the region 2 with time-averaged value of the volume-averaged results.

value of the volume-averaged results. The values of all parameters are the same as in Table I except for the current parameters in the figure. Similar to the trend of the local particle concentration, the coefficient of friction C_P decreases with increasing water inlet velocity. The rate of reduction of the friction coefficient is first fast and then slows, and finally, C_P tends to be a constant value [Fig. 16(a)]. The turning point of the friction coefficient curve is still at the water inlet velocity of approximately 2–3 m/s. From the perspective of reducing the energy loss in the hydraulic lifting process, it is also appropriate to take the water inlet velocity approximately 2–3 m/s. The variation of C_P at different particle inlet concentrations is shown in Fig. 16(b). With the increase in particle inlet concentration, the friction coefficient increases slightly. The smaller the water inlet velocity, the greater the effect of particle inlet concentration on the friction coefficient. This is because the probability of collision between particles and the frequency of collision between particles and the wall increases with the increase in particle inlet concentration, which results in the increase in energy loss. The friction coefficient increases with the increase in the particle density [as shown in Fig. 16(c)]. Hence, higher particle density results in more energy loss. The variance of particle size is also not influential to the friction coefficient [Fig. 16(d)].

Similar analysis at the beginning of Sec. V C is taken, and the friction coefficient C_P can be expressed as

$$C_P = 8.6\sqrt{\frac{\rho_p}{\rho_f}-1}\left(1-\frac{d}{D}\right)^{15.4}\left(\frac{\sqrt{gd}}{u_0}\right)^{2.3}(1-\alpha_{p0})^{-8.9}, \quad (30)$$

where the correlation coefficient $R^2 = 0.98$. Then, the total hydraulic gradient i_t of the mixture can be calculated as

$$i_t = i_m + i_p = C_P\frac{u_0^2}{2gD} + \alpha_p\left(\frac{\rho_p}{\rho_f}-1\right). \quad (31)$$

To explain the physical meaning of the above equation clearly, Eq. (27) is transformed as follows:

$$\begin{aligned}\frac{\Delta P}{H}\frac{1}{\rho_f g} &= \alpha_p\left(\frac{\rho_p}{\rho_f}-1\right)+\frac{\tau_m}{D}\frac{1}{\rho_f g}\\ &= \alpha_p\left(\frac{\rho_p}{\rho_f}-1\right)+C_P\frac{u_0^2}{2gD}.\end{aligned} \quad (32)$$

Equation (31) is equivalent to Eq. (32), that is, the pressure gradient of solid–liquid two-phase flow in the vertical pipe is expressed in terms of the height of the water column. Xia *et al.*[59] built an experimental apparatus to investigate particle settling, particle fluidization, and hydraulic lifting process. The diameter of the pipe in the experimental device is 100 mm, and the water is replaced by tap water. The particles are made of cement and slag, with a diameter of 15 mm and a density of 2000 kg/m^3. The pressure gradient in the vertical pipe was measured. Figure 17 shows the comparison between the total hydraulic gradient calculated using Eq. (31) and the experimental results of.[59] Although there are some errors, the overall agreement is good. If the height of the hydraulic lifting is L, the head of the lifting pump needs to be greater than i_tL. Figure 18 gives the variation of the total hydraulic gradient with the water inlet velocity and the particle inlet concentration. The values of physical parameters are the same as those in Table I. The total hydraulic gradient in hydraulic lifting gradually

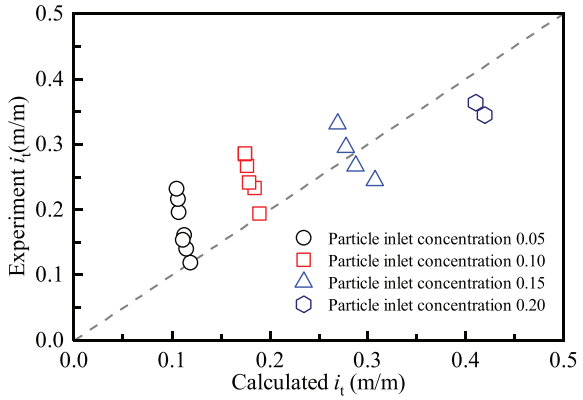

FIG. 17. Comparison between the predicted results and the experimental results[59] of the total hydraulic gradient.

decreases with the increase in the water inlet velocity. The decreasing speed shows a trend of fast and then slows at about 2–3 m/s of the water inlet velocity. In addition, the total hydraulic gradient increases approximately linearly with the increase in particle inlet concentration. The local particle concentration in the vertical pipe also increases with the increase in the inlet particle concentration [Fig. 13(b)], which may result in a risk of pipe clogging. As a result, the inlet particle concentration in field case should not be too large.

D. Flow pattern transition

The flow pattern in vertical and horizontal pneumatic conveying systems is studied in depth now.[65–67] However, little research has been done on the solid–liquid two-phase flow in the vertical pipe. Here, the flow pattern theory in pneumatic conveying is used to analyze the flow pattern transition in this article. Traditionally, the flow patterns can be divided into two main groups: dilute and dense. The dense flow pattern is usually divided into specific flow patterns such as slugging, bubbling, fluidizing, and pluging. Each of these flow patterns might occur for a wide range of flow conditions during the process of a specific conveying system. Figure 19 summarizes all possible flow patterns for the gas-solid two phase flow in the vertical pipe. The Reynolds number and Archimedes number can be used for the transition velocity attributed to vertical two-phase systems. The Reynolds number is a power function of the Archimedes number at the transition of flow patterns.[66] The formula is as follows:

$$Re = mAr^n, \quad (33)$$

where $Re = \rho_f u_0 d/\mu_f$ is the Reynolds number defined in Eq. (19), $Ar = g\rho_f(\rho_p-\rho_f)d^3/\mu_f^2$ is the Archimedes number and can also be written as $(\rho_p/\rho_f-1)Re^2Fr^2$, $Fr = \sqrt{gd/u_0^2}$ is the Froude number defined in Eq. (19). The dense-dilute flow pattern of the solid–liquid two-phase flow in this paper is similar to the flow pattern of slug flow or turbulent fluidization in gas–solid flow as show in Fig. 19. According to the research of Rabinovich and Kalman,[65] the transition velocity attributed to gas–solid conveying might be coupled with the equivalent transition velocity of fluidized bed systems to take into account the solid concentration. Then, the Reynolds number is modified as, which can give better prediction of the flow pattern transition,

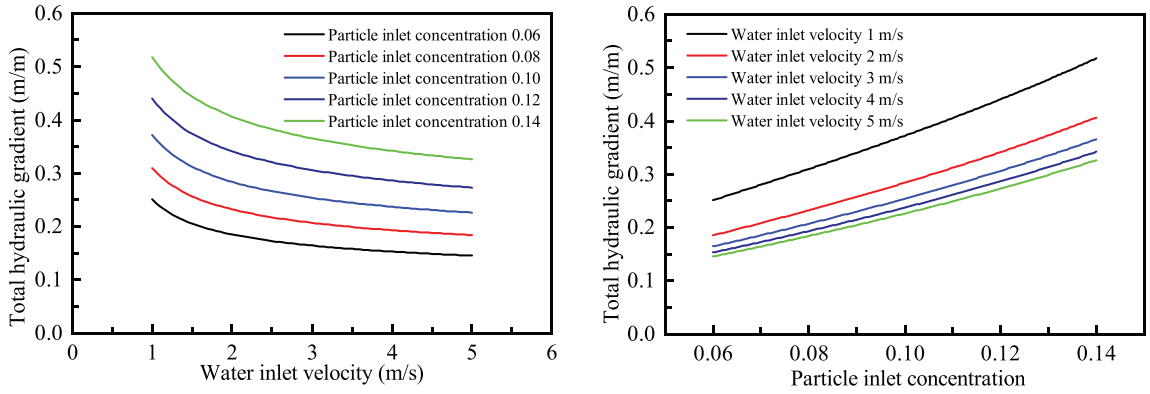

FIG. 18. Change of the total hydraulic gradient with (a) water inlet velocity and (b) particle inlet concentration.

$$Re^* = Re\left[1 - \frac{\varepsilon}{1-\varepsilon}\frac{\alpha_{p0}}{1-\alpha_{p0}}\right], \tag{34}$$

where ε is void fraction and can be calculated by $1 - \alpha_{p,l}$, $\alpha_{p,l}$ is the local particle concentration.

At the transition between the slug flow and the dilute group flows (cluster flow, annular flow, and suspension flow), the following power law relationship was achieved:[65]

$$Re^* = 0.75Ar^{0.56}. \tag{35}$$

Equation (35) can be written as

$$\frac{\rho_f u_{0,tr} d}{\mu_f}\left[1 - \frac{\varepsilon}{1-\varepsilon}\frac{\alpha_{p0}}{1-\alpha_{p0}}\right] = 0.75\left[\frac{g\rho_f(\rho_p - \rho_f)d^3}{\mu_f^2}\right]^{0.56}, \tag{36}$$

where $u_{0,tr}$ is the transition velocity. From Fig. 11(a), the local particle concentration is around 0.08–0.14 with the particle inlet concentration α_{p0} of 0.08. Hence, the void fraction ε is set as 0.88. All parameters in Eq. (36) have the same values as in Table I. The transition velocity $u_{0,tr}$ is calculated as 2.24 m/s. Then, when the water inlet velocity is approximately 2.24 m/s, the solid–liquid two-phase flow in the vertical pipe changes the flow pattern. In general, the transition between the slug flow and the dilute group flows is characterized by rapid decrease in the local particle concentration with increasing water inlet velocity.[65,68,69] The transition from the dense-dilute flow pattern to the dilute group flow pattern may happen at the point where the local particle concentration decreases from fast to slow. As a result, the transition velocity is around 2–3 m/s [as shown in Fig. 13(a)]. The modified Reynolds number Re^* is approximately 12 000 at this condition.

VI. CONCLUSION

In this work, an optimized Eulerian–Lagrangian method is utilized for investigating dense coarse particle transportation in a vertical pipe, which is a typical process of the hydraulic lifting in deep-sea mining. The in-house codes of the Eulerian–Lagrangian method are algorithmically implanted in the open-source FVM tools OpenFOAM and are validated in this work. The problem of particle transportation process in a vertical pipe is proposed and formulated. Various groups of cases are designed to elucidate the process. Embedded physical mechanisms are comprehensively discussed to provide deeper insights, and quantitative correlation curves are obtained for the critical lifting condition and hydraulic gradient.

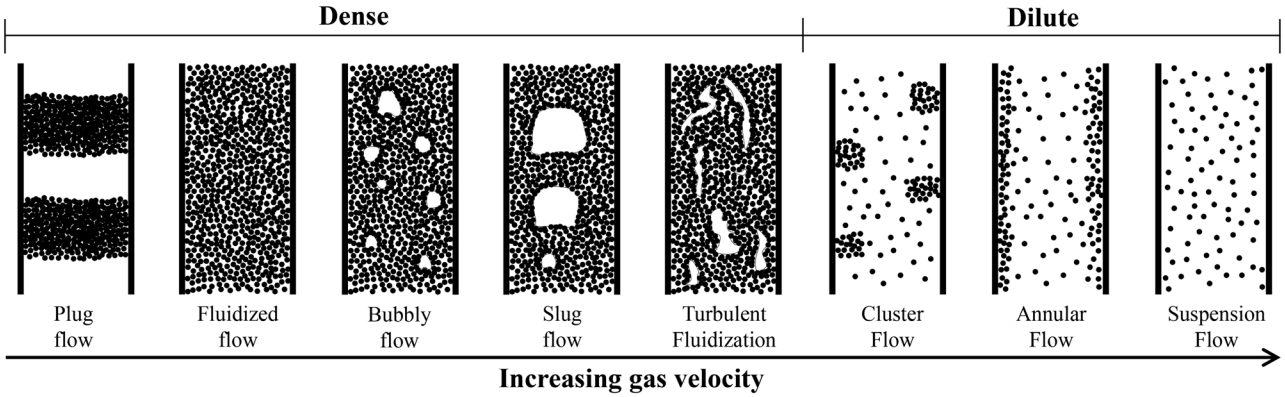

FIG. 19. Schematics of different flow patterns for the gas–solid two phase flow in a vertical pipe.

(i) The movement characteristics of particles such as particle concentration and particle velocity in the vertical pipe are obtained. According to the time-varying curve trend of the particle concentration and combined with the numerical results, the particle transportation process in the vertical pipe can be roughly divided into three stages: single phase flow stage (stage I), mixing stage (stage II), and stable transportation stage (stage III). The single phase flow stage and the mixing stage only take up a small part of the whole time. Hence, we focus on the stable transportation stage. During the stable transportation stage, the time series of value such as the particle concentration is pulsating, which may result from the turbulence irregularity of the water movement, the dynamic change of the force on the particles caused by the change of the particle concentration, and collisions between particles. In addition, the particles show a dense-dilute flow pattern in the vertical pipe due to the particle retention and the particle size segregation. The particle retention results from the density difference between the particles and water and is detailed analyzed under different conditions. (ii) The water inlet water velocity and inlet particle concentration have a great influence on hydraulic lifting. The particle retention phenomenon alleviates with the increase in the water inlet velocity and almost disappears when the water inlet velocity is larger than 3 m/s. The large inlet particle concentration may promote the occurrence of clogging. (iii) The non-dimensional relationship between the relative particle vertical velocity and other parameters such as the Froude number and the density ratio is obtained based on the dimensional analysis and analogous analysis of the particle settling process. Two formulas for predicting the critical hydraulic lifting velocity and the total hydraulic gradient, respectively, are given and proven. In order to balance the stability and economy of hydraulic lifting for deep-sea mining, it is recommended to control the water inlet velocity at approximately 2–3 m/s and the inlet particle concentration at approximately 0.01. Based on the flow pattern transition in this work, the flow pattern of the solid–liquid and the gas–solid two-phase flow may be different. In our future work, the flow pattern of the solid-liquid two-phase flow will be investigated in depth.

ACKNOWLEDGMENTS

This study was supported by the Strategic Priority Research Program of the Chinese Academy of Sciences (Grant No. XDA22000000), the National Natural Science Foundation of China (Grant No. 12132018), and the Youth Innovation Promotion Association of Chinese Academy of Sciences (No. 2017027).

AUTHOR DECLARATIONS

Conflict of Interest

The authors have no conflicts to disclose.

DATA AVAILABILITY

The data that support the findings of this study are available from the corresponding author upon reasonable request.

REFERENCES

[1]J. Wang, D. Elsworth, and M. K. Denison, "Propagation, proppant transport and the evolution of transport properties of hydraulic fractures," J. Fluid Mech. **855**, 503–534 (2018).
[2]J. Zeng, P. Tang, H. Li, and D. Zhang, "Simulating particle settling in inclined narrow channels with the unresolved CFD-DEM method," Phys. Rev. Fluids **6**, 034302 (2021).
[3]T. Trewhela, J. M. N. T. Gray, and C. Ancey, "Large particle segregation in two-dimensional sheared granular flows," Phys. Rev. Fluids **6**, 054302 (2021).
[4]Y. Dai, Y. Zhang, and X. Li, "Numerical and experimental investigations on pipeline internal solid–liquid mixed fluid for deep ocean mining," Ocean Eng. **220**, 108411 (2021).
[5]H. Zhang, T. Li, Z. Huang, S. Kuang, and A. Yu, "Investigation on vertical plug formation of coarse particles in a non-mechanical feeder by CFD-DEM coupling method," Powder Technol. **332**, 79–89 (2018).
[6]M. Zhou, S. Wang, S. Kuang, K. Luo, J. Fan, and A. Yu, "CFD-DEM modelling of hydraulic conveying of solid particles in a vertical pipe," Powder Technol. **354**, 893–905 (2019).
[7]X. Ting, Z. Xinzhuo, S. A. Miedema, and C. Xiuhan, "Study of the characteristics of the flow regimes and dynamics of coarse particles in pipeline transportation," Powder Technol. **347**, 148–158 (2019).
[8]S. Kuang, M. Zhou, and A. Yu, "CFD-DEM modelling and simulation of pneumatic conveying: A review," Powder Technol. **365**, 186–207 (2020).
[9]Y. Zhang, X. Lu, X. Zhang, Y. Chen, H. Xiong, and L. Zhang, "Experimental investigation of critical suction velocity of coarse solid particles in hydraulic collecting," Acta Mech. Sin. **37**, 613–617 (2021).
[10]E. A. Schnorr Filho, N. C. Lima, and E. M. Franklin, "Resolved CFD-DEM simulations of the hydraulic conveying of coarse grains through a very-narrow elbow," Powder Technol. **395**, 811–821 (2022).
[11]X. Zhang, X. Lu, and L. Liu, "Advances in natural gas hydrate recovery methods," Prog. Geophys. **29**, 858–869 (2014) (in Chinese).
[12]P. Li, X. Zhang, and X. Lu, "Three-dimensional Eulerian modeling of gas–liquid–solid flow with gas hydrate dissociation in a vertical pipe," Chem. Eng. Sci. **196**, 145–165 (2019).
[13]P. Li, X. Zhang, and X. Lu, "Dissociation equilibrium height and friction coefficient in pipeline transportation of gas hydrate-bearing sediment particles," J. Nat. Gas Sci. Eng. **81**, 103470 (2020).
[14]C. L. Lopes, L. Bastos, M. Caetano, I. Martins, M. M. Santos, and I. Iglesias, "Development of physical modelling tools in support of risk scenarios: A new framework focused on deep-sea mining," Sci. Total Environ. **650**, 2294–2306 (2019).
[15]G. Zhao, L. Xiao, Z. Yue, M. Liu, T. Peng, and W. Zhao, "Performance characteristics of nodule pick-up device based on spiral flow principle for deep-sea hydraulic collection," Ocean Eng. **226**, 108818 (2021).
[16]J. van Wijk and E. de Hoog, "Size reduction of ccz polymetallic nodules under repeated impact fragmentation," Results Eng. **7**, 100154 (2020).
[17]F. D. Cúñez, N. C. Lima, and E. M. Franklin, "Motion and clustering of bonded particles in narrow solid–liquid fluidized beds," Phys. Fluids **33**, 023303 (2021).
[18]F. D. Cúñez and E. M. Franklin, "Crystallization and jamming in narrow fluidized beds," Phys. Fluids **32**, 083303 (2020).
[19]A. Bartosik, "Validation of friction factor predictions in vertical slurry flows with coarse particles," J. Hydrol. Hydromech. **68**, 119–127 (2020).
[20]M. Sakai, H. Takahashi, C. C. Pain, J.-P. Latham, and J. Xiang, "Study on a large-scale discrete element model for fine particles in a fluidized bed," Adv. Powder Technol. **23**, 673–681 (2012).
[21]K. J. Dong, R. Yang, R. Zou, and A. Yu, "Settling of particles in liquids: Effects of material properties," AIChE J. **58**, 1409–1421 (2012).
[22]M. Sakai, M. Abe, Y. Shigeto, S. Mizutani, H. Takahashi, A. Viré, J. R. Percival, J. Xiang, and C. C. Pain, "Verification and validation of a coarse grain model of the DEM in a bubbling fluidized bed," Chem. Eng. J. **244**, 33–43 (2014).
[23]B. Blais and F. Bertrand, "On the use of the method of manufactured solutions for the verification of CFD codes for the volume-averaged Navier–Stokes equations," Comput. Fluids **114**, 121–129 (2015).
[24]V. Jain, L. Kalo, D. Kumar, H. J. Pant, and R. K. Upadhyay, "Experimental and numerical investigation of liquid–solid binary fluidized beds: Radioactive particle tracking technique and dense discrete phase model simulations," Particuology **33**, 112–122 (2017).
[25]C. Fernandes, D. Semyonov, L. Ferrás, and J. Nobrega, "Validation of the CFD-DPM solver DPMFoam in OpenFOAM® through analytical, numerical and experimental comparisons," Granular Matter **20**, 18 (2018).

[26]P. Vlasák, Z. Chára, V. Matoušek, J. Konfršt, and M. Kesely, "Experimental investigation of fine-grained settling slurry flow behaviour in inclined pipe sections," J. Hydrol. Hydromech. **67**, 113–120 (2019).
[27]P. Vlasák, V. Matoušek, Z. Chára, J. Krupička, J. Konfršt, and M. Kesely, "Concentration distribution and deposition limit of medium-coarse sand-water slurry in inclined pipe," J. Hydrol. Hydromech. **68**, 83–91 (2020).
[28]L. Liu, J. Yang, H. Lu, X. Tian, and W. Lu, "Numerical simulations on the motion of a heavy sphere in upward Poiseuille flow," Ocean Eng. **172**, 245–256 (2019).
[29]L. Zou, J. Z. Sun, Z. Sun, Z. B. Yu, and H. B. Zhao, "Study of two free-falling spheres interaction by coupled SPH–DEM method," Eur. J. Mech.—B/Fluids **92**, 49–64 (2022).
[30]W. Chen, H.-L. Xu, W.-Y. Kong, and F. Q. Yang, "Study on three-phase flow characteristics of natural gas hydrate pipeline transmission," Ocean Eng. **214**, 107727 (2020).
[31]Q. Chen, T. Xiong, X. Zhang, and P. Jiang, "Study of the hydraulic transport of non-spherical particles in a pipeline based on the CFD-DEM," Eng. Appl. Comput. Fluid Mech. **14**, 53–69 (2020).
[32]S. Masanobu, S. Takano, T. Fujiwara, S. Kanada, M. Ono, and H. Sasagawa, "Study on hydraulic transport of large solid particles in inclined pipes for subsea mining," J. Offshore Mech. Arct. Eng. **139**, 051401 (2017).
[33]H. Xu, W. Kong, and F. Yang, "Decomposition characteristics of natural gas hydrates in hydraulic lifting pipelines," Nat. Gas Ind. B **6**, 159–167 (2019).
[34]J. Van Wijk, F. Van Grunsven, A. Talmon, and C. van Rhee, "Simulation and experimental proof of plug formation and riser blockage during vertical hydraulic transport," Ocean Eng. **101**, 58–66 (2015).
[35]J. Van Wijk, A. Talmon, and C. van Rhee, "Stability of vertical hydraulic transport processes for deep ocean mining: An experimental study," Ocean Eng. **125**, 203–213 (2016).
[36]S. Sundaresan, A. Ozel, and J. Kolehmainen, "Toward constitutive models for momentum, species, and energy transport in gas–particle flows," Annu. Rev. Chem. Biomol. Eng. **9**, 61–81 (2018).
[37]Y. Zhang, X.-B. Lu, and X.-H. Zhang, "An optimized Eulerian–Lagrangian method for two-phase flow with coarse particles: Implementation in open-source field operation and manipulation, verification, and validation," Phys. Fluids **33**, 113307 (2021).
[38]W. D. Fullmer, G. Liu, X. Yin, and C. M. Hrenya, "Clustering instabilities in sedimenting fluid–solid systems: Critical assessment of kinetic-theory-based predictions using direct numerical simulation data," J. Fluid Mech. **823**, 433–469 (2017).
[39]G. Tronci, A. Buffo, M. Vanni, and D. Marchisio, "Validation of the diffusion mixture model for the simulation of bubbly flows and implementation in OpenFOAM," Comput. Fluids **227**, 105026 (2021).
[40]J. Wang, X. Chen, W. Bian, B. Zhao, and J. Wang, "Quantifying the non-equilibrium characteristics of heterogeneous gas–solid flow of smooth, inelastic spheres using a computational fluid dynamics–discrete element method," J. Fluid Mech. **866**, 776–790 (2019).
[41]Y. Zhang, X. Lu, X. Zhang, and P. Li, "Numerical simulation on flow characteristics of large-scale submarine mudflow," Appl. Ocean Res. **108**, 102524 (2021).
[42]P. Sippola, J. Kolehmainen, A. Ozel, X. Liu, P. Saarenrinne, and S. Sundaresan, "Experimental and numerical study of wall layer development in a tribo-charged fluidized bed," J. Fluid Mech. **849**, 860–884 (2018).
[43]P. A. Cundall and O. D. L. Strack, "A discrete numerical model for granular assemblies," Géotechnique **29**, 47–65 (1979).
[44]H. Kuo, P. Knight, D. Parker, Y. Tsuji, M. Adams, and J. Seville, "The influence of DEM simulation parameters on the particle behaviour in a V-mixer," Chem. Eng. Sci. **57**, 3621–3638 (2002).
[45]E. Berberović, N. P. van Hinsberg, S. Jakirlić, I. V. Roisman, and C. Tropea, "Drop impact onto a liquid layer of finite thickness: Dynamics of the cavity evolution," Phys. Rev. E **79**, 036306 (2009).
[46]H. Jasak, "Error analysis and estimation for the finite volume method with applications to fluid flows," Ph.D. thesis (Imperial College London, University of London, 1996).
[47]D. Li and H. Christian, "Simulation of bubbly flows with special numerical treatments of the semi-conservative and fully conservative two-fluid model," Chem. Eng. Sci. **174**, 25–39 (2017).
[48]J. J. Derksen, H. E. A. van den Akker, and S. Sundaresan, "Two-way coupled large-eddy simulations of the gas-solid flow in cyclone separators," AIChE J. **54**, 872–885 (2008).
[49]M. Zhou, S. Kuang, K. Luo, R. Zou, S. Wang, and A. Yu, "Modeling and analysis of flow regimes in hydraulic conveying of coarse particles," Powder Technol. **373**, 543–554 (2020).
[50]M. Zhou, S. Kuang, F. Xiao, K. Luo, and A. Yu, "CFD-DEM analysis of hydraulic conveying bends: Interaction between pipe orientation and flow regime," Powder Technol. **392**, 619–631 (2021).
[51]D. Gidaspow, *Multiphase Flow and Fluidization: Continuum and Kinetic Theory Descriptions* (Academic Press, San Diego, 1994).
[52]P. Traoré, J.-C. Laurentie, and L. Dascalescu, "An efficient 4 way coupling CFD–DEM model for dense gas–solid particulate flows simulations," Comput. Fluids **113**, 65–76 (2015).
[53]Y. Li, S. Liu, and X. Hu, "Research on rotating speed's influence on performance of deep-sea lifting motor pump based on DEM-CFD," Mar. Georesour. Geotechnol. **37**, 979–988 (2019).
[54]Y. Televantos, C. Shook, M. Streat, and A. Carleton, "Flow of slurries of coarse particles at high solids concentrations," Can. J. Chem. Eng. **57**, 255–262 (1979).
[55]A. Farzanegan, N. Khorasanizadeh, G. Sheikhzadeh, and H. Khorasanizadeh, "Laboratory and CFD investigations of the two-phase flow behavior in flotation columns equipped with vertical baffle," Int. J. Miner. Process. **166**, 79–88 (2017).
[56]H. Yang and S. Liu, "Measuring method of solid-liquid two-phase flow in slurry pipeline for deep-sea mining," Thalassas **34**, 459–469 (2018).
[57]D. C. Rapaport, *The Art of Molecular Dynamics Simulation*, 2nd ed. (Cambridge University Press, New York, 2004).
[58]G. Capodaglio and E. Aulisa, "A particle tracking algorithm for parallel finite element applications," Comput. Fluids **159**, 338–355 (2017).
[59]J. Xia, J. Ni, and C. Mendoza, "Hydraulic lifting of manganese nodules through a riser," J. Offshore Mech. Arct. Eng. **126**, 72–77 (2004).
[60]Q. Tan, *Dimensional Analysis with Case Studies in Mechanics* (Springer-Verlag, Berlin/Heidelberg, 2011).
[61]P. Li, "Studies on mechanism of hydraulic hoist of coarse particle in vertical pipe," Ph.D. thesis (Tsinghua University, 2007) (in Chinese).
[62]W. Jin, X. Huang, and W. Gao, "An experimental study on minimal transporting velocity of the lifted large-size particle material in vertical piping," Min. Res. Dev. **17**, 17–20 (1997) (in Chinese).
[63]M. LaViolette, "On the History, Science, and Technology Included in the Moody Diagram," J. Fluids Eng. **139**, 030801 (2017).
[64]A. L. Ferre and C. A. Shook, "Coarse particle wall friction in vertical slurry flows," Part. Sci. Technol. **16**, 125–133 (1998).
[65]E. Rabinovich and H. Kalman, "Flow regime diagram for vertical pneumatic conveying and fluidized bed systems," Powder Technol. **207**, 119–133 (2011).
[66]X. Cong, X. Guo, H. Lu, X. Gong, K. Liu, X. Sun, and K. Xie, "Flow patterns of pulverized coal pneumatic conveying and time-series analysis of pressure fluctuations," Chem. Eng. Sci. **101**, 303–314 (2013).
[67]A. Bougouin, L. Lacaze, and T. Bonometti, "Collapse of a liquid-saturated granular column on a horizontal plane," Phys. Rev. Fluids **4**, 124306 (2019).
[68]I. A. Costa, M. Do Carmo. Ferreira, and J. T. Freire, "Analysis of regime transitions and flow instabilities in vertical conveying of coarse particles using different solids feeding systems," Can. J. Chem. Eng. **82**, 48–59 (2008).
[69]Ž. B. Grbavčić, R. V. Garić-Grulović, and Z. L. Arsenijević, "Prediction of the choking velocity and voidage in vertical pneumatic conveying of coarse particles," Powder Technol. **161**, 1–9 (2006).